Am J Nucl Med Mol Imaging 2019;9(6):321-334
www.ajnmmi.us /ISSN:2160-8407/ajnmmi0104822

Original Article

Dynamic monitoring of STAT3 activation in live cells using a novel STAT3 Phospho-BRET sensor

Shalini Dimri[1,2], Rohit Arora[1], Akshi Jasani[1], Abhijit De[1,2]

[1]*Molecular Functional Imaging Lab, Advanced Centre for Treatment, Research and Education in Cancer, Tata Memorial Centre, Navi Mumbai, India;* [2]*Department of Life Sciences, Homi Bhabha National Institute, Mumbai, India*

Received November 12, 2019; Accepted December 11, 2019; Epub December 15, 2019; Published December 30, 2019

Abstract: Phosphorylation (pY705) mediated homodimerization is a rate-limiting step controlling STAT3 key oncogenic functions making it an attractive target for drug discovery. Hence, this study reports development of a sensitive and versatile STAT3 Phospho-BRET biosensor platform technology to monitor activation dynamics of STAT3 signalling directly from live cells. Categorically, we first demonstrate that NanoLuc donor and TurboFP635 acceptor serves as an excellent BRET system over other tested fluorophores like mOrange and TagRFP, both for live cells as well as *in vivo* optical imaging of protein-protein interactions. Based on initial multi-parametric optimizations, our Phospho-BRET sensor developed by fusing STAT3 with NanoLuc and TurboFP at the C-terminus, successfully captured the activation kinetics of STAT3 in response to different ligands (e.g. IL6 & EGF) and across multiple cancer cell types either with or without the endogenous STAT3 pool. Perturbation in EGF-mediated STAT3 BRET activation signal upon blocking with EGFR neutralizing antibody further confirms the specificity of the sensor to judge ligand-receptor pathway dependent STAT3 activation. Finally, we determine the high-throughput compatibility of the developed biosensor by testing a few known/unknown STAT3 inhibitors in a 96- and 384-well plate format. The results from this screen revealed that drug molecules such as curcumin and niclosamide are more efficient inhibitors over known molecule like Stattic. Thus, the STAT3 Phospho-BRET sensor is a first of its kind live cell platform technology developed for its use to study STAT3 pathway dynamics and screen potential drug molecules *in vivo*.

Keywords: Bioluminescence resonance energy transfer (BRET), nanoluciferase, TurboFP635, phosphorylation, STAT3, cancer, high-throughput screening, protein-protein interactions, niclosamide, Stattic

Introduction

Complex cellular behaviour in response to a wide variety of external stimuli is a highly regulated and controlled process driven by multiple protein-protein interactions (PPIs) [1]. Although numerous assays are available for detecting PPIs, capturing these interactions in a cellular context is still a challenging task [2]. Bioluminescence resonance energy transfer (BRET) is an attractive assay primarily used for monitoring PPIs and/or temporal conformational changes in natural cellular environment. It is a proximity dependent assay, where non-radiative energy from donor luciferase-substrate reaction is transferred to excite the acceptor-fluorophore typically located within 0-10 nm of physiological distance. Due to the enzymatic nature of the donor molecule, no external illumination is required, and thus this assay offers high signal to background ratio with excellent sensitivity [3]. Recently, several high quantum efficient luciferase or luciferase variants were reported [4]. One such key luciferase molecule is NanoLuc (Nluc), which is the smallest known (19 KDa), ATP-independent luciferase producing highest photon flux known so far [5]. Because of its high quantum efficiency, NanoLuc-based system has been utilized for several potential applications, including monitoring protein stability [6], protein-protein interactions (GPCRs, NanoBRET) [7, 8], protein-ligand interactions (Epo-Epo receptor, INSL3-RXFP2) [9, 10] as well as gene regulation and cell signalling [11, 12].

STAT3 is a key oncogenic signalling molecule primarily activated by pY705 phosphorylation

leading to its homodimerization and nuclear translocation, where it acts as a potent transcription factor for its target genes [13]. Pertaining to its essential role as an oncogenic player, identifying drugs through virtual screening of inhibitor library is a mainstay approach [14]. Subsequently, efforts have been made in the past to develop study methodology for detecting STAT3 activation in live cells [15]. There are reports on a synthetic optical reporter for Y705 residue (Trp564 mutated to 7-hydroxycoumarin-4-yl) [16]. A FRET-based sensor has also been used to study localization dynamics of STAT3 in live cells using CFP and YFP as partners [17]. However, pertaining to low sensitivity and lack of unified assay system for *in vitro* and *in vivo* validation, none of the methods developed so far, have shown potential to study perturbations in STAT3 signalling dynamics or screen potential inhibitors in a high-throughput format from living system.

Hence, the present study is an effort to develop a highly sensitive protein phosphorylation biosensor using BRET platform technology for deciphering live cell STAT3 dimerization kinetics as an oncogenic candidate. Further, we have also attempted to demonstrate high-throughput screening (HTS) compatibility of this sensor for judging inhibitory action of drugs against STAT3 pathway.

Materials and methods

Materials

EGF (#AF-100-15) and IL6 (#200-06) were bought from Peprotech (USA). NanoLuc plasmid and anti-Nluc antibody were provided as a generous gift from Promega. Anti–total STAT3 (#9139), anti-pY705 STAT3 (#D3A7), anti-EGFR blocking antibody (#54359) were from Cell signalling (USA). Anti-RFP antibody [RF5R] (ab12-5244), anti-mouse-HRP (#ab6728) from Abcam and anti-rabbit-HRP (#31460) from Invitrogen. Furimazine (#N1110) was from Promega and Lipofectamine 2000 (#11668019) reagent was from Thermo Fischer. Coelenterazine (native, #C-7001) was purchased from Biosynth International (Switzerland). Stattic (#S7024) was purchased from Selleckchem (USA). CI-994 (#1742), AR-42 (#2716), Chidamide (#2261) and MS-275 (#1590) were from Biovision (USA). Niclosamide (#N3510) and Curcumin (#08511) were from Sigma (USA). BRET measurements were done using IVIS Spectrum In Vivo Imaging System from Perkin Elmer (USA) equipped with filters ranging from 500-850 nm with 20 nm bandwidth and Cytation Imaging reader from Biotek (USA) with filter range from 400-680 nm and band pass of 20 nm.

Plasmid preparation

Fusion constructs of full length nanoluciferase (Nluc) with different fluorophores were prepared in a pCMV empty vector containing suitable flexible GGSGGS repeat linker. The Nluc gene was inserted at the C-terminus by cloning a PCR amplified (516 base pairs) full length sequence using XhoI and BamHI restriction sites while PCR amplified fluorophores (TurboFP, TagRFP and mOrange) were inserted at N-terminus without stop codon using EcoRI and BglII restriction sites. A linker length of 12 amino acids was maintained between the fusion gene sequences. For dipole orientation related studies, PCR amplified fragment of XhoI-mOrange-BamHI was cloned at the C-terminus of pCMV-GGS vector while Nluc was inserted at the N-terminus using EcoRI and BglII restriction sites separated by a linker of 12 amino acids. mOrange-Nluc (12 a.a.) fusion construct was prepared as above. Optimization of linker length was achieved by ligating EcoRI-mOrange-BglII at the N-terminus and XhoI-Nluc-BamHI at the C-terminus in pCMV vector containing GGS linker of length varying from 12 a.a., 18 a.a. to 24 a.a. For achieving a separation of 9 a.a. linker length, mOrange was inserted using NheI and HindIII restriction sites while Nluc containing stop codon was amplified and ligated with AgeI and BamHI sites.

Expression vectors pSTAT3-Nluc and pSTAT3-TurboFP were prepared by amplifying full length STAT3 sequence from STAT3 (Y705F)-TAL-Luc plasmid (gift from Afshin Dowlati, Addgene plasmid # 46933) [18] flanked by NheI and SalI restriction sites and inserting into pCMV-GGS-Nluc and pCMV-GGS-TurboFP vectors (10 a.a. linker separation) at the N-terminus. pNluc-STAT3 and pTurbo-STAT3 expression vectors were prepared by inserting PCR amplified XhoI-STAT3 (Y705F)-BamHI sequence with stop codon into the C-terminus of pNluc-GGS and pTurboFP-GGS vector with linker separation of 12 a.a. Mutant STAT3 (Y705F) was converted to wild type sequence by site-directed muta-

genesis (Forward primer: 5' AGCGCTGCCCCATACCTGAAGACC 3', reverse primer: 5' GGTCTTCAGGTATGGGGCAGCGCT 3') in all relevant constructs.

Cell culture and transfection

HT1080 and PC3 cells were cultured in DMEM medium (Gibco, USA) supplemented with 10% fetal bovine serum (Gibco, USA) and 1% penicillin/streptomycin (Invitrogen, USA). A549 and MCF7 cells were maintained in RPMI1640 (Gibco, USA) supplemented with 10% fetal bovine serum (Gibco, USA) and 1% penicillin/streptomycin (Invitrogen, USA). All cells were maintained at 37°C in a 5% CO_2 humidified atmosphere. One day prior to transfection 1×10^5 cells were seeded in a 12 well-flat bottom plate. Transfection was carried out at an optimal confluency of 80% using Lipofectamine 2000 transfection reagent as per manufacturer's instructions. For BRET studies expression vectors coding for donor and acceptor plasmid were transfected in 1:1 ratio. Post-transfection medium was replaced and cells were maintained in normal culture condition until used.

Acceptor stable cells were developed by transfecting TurboFP-STAT3 or STAT3-TurboFP plasmids in HT1080 cells followed by antibiotic selection of stable clones using Zeocin (Invitrogen) (500 µg/ml).

Immunoblotting

Briefly cells were suspended in lysis buffer containing 10 mM Tris-HCl (pH 7.5), 140 mM NaCl, 5 mM EDTA, 2 mM EGTA, 100 mM NaF, 100 mM Na_3VO_4, 100 mM PMSF and protease inhibitor cocktail. The mixture was lysed using sonicator and centrifuged at 14000 rpm for 30 min at 4°C. Supernatant was collected and protein estimation was done using Bradford reagent (Sigma, USA). Samples were prepared in 1× Laemmli buffer and boiled at 95°C for 3 mins. Protein samples (50-60 µg) were separated in 10% SDS-PAGE gel and transferred onto nitrocellulose membrane using semi-dry transfer assembly (15 V for 1 hr), followed by incubation with blocking buffer (5% non-fat dry milk in 1XTBS and 0.1% Tween 20) for 1 hr. The blots were incubated with primary antibody at a relevant dilution (anti-STAT3 1:1000, anti-pY705 STAT3 1:500, anti-NanoLuc 1:1000 and anti-RFP 1:1000) overnight at 4°C. Next day, blots were processed for incubation with HRP conjugated-secondary antibody (1:10,000 dilution) for 1 hr. Chemiluminescence signal was captured using ECL substrate in ChemiDoc system (Biorad, USA).

Quantitative real time PCR

Total RNA was extracted using RNA extraction minikit (QIAGEN) followed by cDNA preparation from 2 µg RNA using SuperScript III (Invitrogen) kit. Normalization was performed using GAPDH as internal control. Primer sequence for EGFR and GAPDH is as follows: EGFR Fwd: 5' AGGCACAAGTAACAGGCTCAC; EGFR Rev: 5' AAGGTCGTAATTCCTTTGCAC; GAPDH Fwd: 5' TGCACCACCAACTGCTTAGC; GAPDH Rev: 5' GGCATGGACTGTGGTCATGAG.

Fluorescence microscopy

HT1080 cells stably expressing the pCMV-STAT3-TurboFP and pCMV-TurboFP-STAT3 constructs were seeded on cover slips and fixed with 4% paraformaldehyde for 10 min at 37°C. DAPI was used for nuclear staining and images were acquired using Zeiss LSM 780 Confocal Microscope (Germany) with 633 nm filter for TurboFP635 and 460 nm for DAPI.

BRET imaging and analysis

24 hrs post transfection, cells expressing donor alone and donor-acceptor fusion constructs were trypsinized and seeded in a 96 black well plate with clear bottom. Cells were allowed to adhere overnight at 37°C with 5% CO_2. For BRET studies, 50 ul furimazine (1:1000 diluted in DMEM from main stock) was added to each well and acquisition was performed in IVIS spectrum. Emission spectra were captured from 500-680 nm with an integration time of 1 s/filter and 20 nm step increments.

For monitoring functionality of the STAT3 phosphorylation sensor, 24 hrs post transfection, donor alone and donor-acceptor co-transfected cells (20,000 cells/well in 96 and 5000 cells/well for 384 well format) were distributed in black well plates in serum-negative medium. After 24 hrs of serum starvation, cells were triggered with STAT3 pathway ligands (IL6 or EGF) in varying concentrations (5 ng-10 ng IL6, 10-100 ng EGF) reconstituted in serum-negative medium followed by addition of 50 ul

furimazine/well (1:1000 diluted). To study the effect of inhibitors on STAT3 activation, cells were first incubated with varying concentrations of different inhibitors for 24 hrs followed by EGF (100 ng) and substrate addition. For Ab blocking study, cells were preincubated with EGFR blocking antibody for 4 hrs (1:100 dilution) and then EGF (100 ng) along with luciferase substrate was added. One set was left untreated as control group. For all BRET analyses, ROIs were drawn on each well and Average Radiance was calculated in both donor channel (500 nm) and acceptor channel (580 nm-mOrange, 600 nm-TagRFP and 640 nm-TurboFP), for donor alone and donor-acceptor samples. Analysis was done in Living image software version 4.5 for IVIS spectrum.

For acquisition done on Cytation 5 Imaging reader, followed by substrate addition, spectral scan was performed from 400 nm to 680 nm keeping 20 nm band pass filter with an integration time of 1 sec/filter for all the samples. The output for each well was measured in Relative light units (RLU) that was further used for calculating BRET ratios.

In order to calculate BRET ratio, following equations were used [4, 19]:

$$\text{BRET Ratio} = \frac{BL_{emission}\ (\text{Acceptor } \lambda)}{BL_{emission}\ (\text{Donor } \lambda)} - \frac{C_f \times BL_{emission}\ (\text{Donor } \lambda)}{BL_{emission}\ (\text{Donor } \lambda)}$$

$$\text{Where, } C_f = \left(\frac{BL_{emission}\ (\text{Acceptor } \lambda)}{BL_{emission}\ (\text{Donor } \lambda)}\right)_{\text{Donor only}}$$

In vivo bioluminescence imaging

All *in vivo* experiments were performed in compliance with the standard protocol of the institutional animal ethics committee (IAEC), ACTREC. For performing *in vivo* BRET, equal number of HT1080 (3×10^6) cells stably expressing either Nluc alone (above) or TurboFP-Nluc fusion protein (bottom) were implanted subcutaneously on to the dorsal right flank of 6-8 weeks old nude mice (N=3). 30 mins post implantation, 100 µl furimazine (1:20 diluted in 1XPBS) was injected via intraperitoneal route and mice were anesthetised using 2.5% (vol/vol) gaseous isoflurane in oxygen. Acquisition was performed in IVIS spectrum equipped with CCD camera at 500 nm for donor channel and 640 nm for acceptor channel with integration time of 60 sec/filter. For calculating double ratio (DR), the following equation was used [20, 21]:

$$DR = \frac{\left(\frac{BL_{acceptor\ channel} \times \mu_t\ (\text{acceptor channel})}{BL_{donor\ channel} \times \mu_t\ (\text{donor channel})}\right)_{(\text{Donor + Acceptor})}}{\left(\frac{BL_{acceptor\ channel} \times \mu_t\ (\text{acceptor channel})}{BL_{donor\ channel} \times \mu_t\ (\text{donor channel})}\right)_{(\text{Donor alone})}}$$

Where, μ_t is total attenuation coefficient. Here, DR is independent of μ_t.

Statistical analysis

For all data analysis student *t*-test (paired and two-sided) was employed. *p*-value<0.05 was considered statistically significant.

Results and discussion

NanoLuc is an efficient donor for BRET partnering with multiple red fluorescent proteins

For successful developing of a BRET based STAT3 Phosphorylation sensor, careful selection of an appropriate acceptor pair with the NanoLuc (Nluc)-donor is essential. Hence, three red fluorescent proteins, i.e. mOrange (Ex_{Max} 548 nm/Em_{Max} 562 nm), TagRFP (Ex_{Max} 555 nm/Em_{Max} 584 nm) or TurboFP (Ex_{Max} 588 nm/Em_{Max} 635 nm) were selected and individually fused to Nluc with a separation of 12 a.a. flexible GGS linker (**Figure 1A**). The integrity of fusion and expression of the above-mentioned BRET pairs was confirmed by immunoblotting and probing with anti-RFP antibody (**Figure 1B**). Transient overexpression of the three BRET pairs in HT1080 cells show that due to its high quantum output, Nluc is able to transfer sufficient energy to excite all the three fluorescence proteins used here, resulting in their characteristic emission maxima detected using appropriate acceptor filters (mOrange-560 nm, TagRFP-580 nm and TurboFP-640 nm) (**Figure 1C**). Further, with decreasing spectral overlap with Nluc emission, TurboFP (322.57 mBU [mBU is milli BRET unit]) and TagRFP (277.79 mBU) always exhibit BRET ratios less than mOrange (460.72 mBU, P<0.001). However, the BRET ratio obtained with Furimazine as substrate for Nluc were always higher in comparison to when only coelenterazine was used [for e.g. mOr-

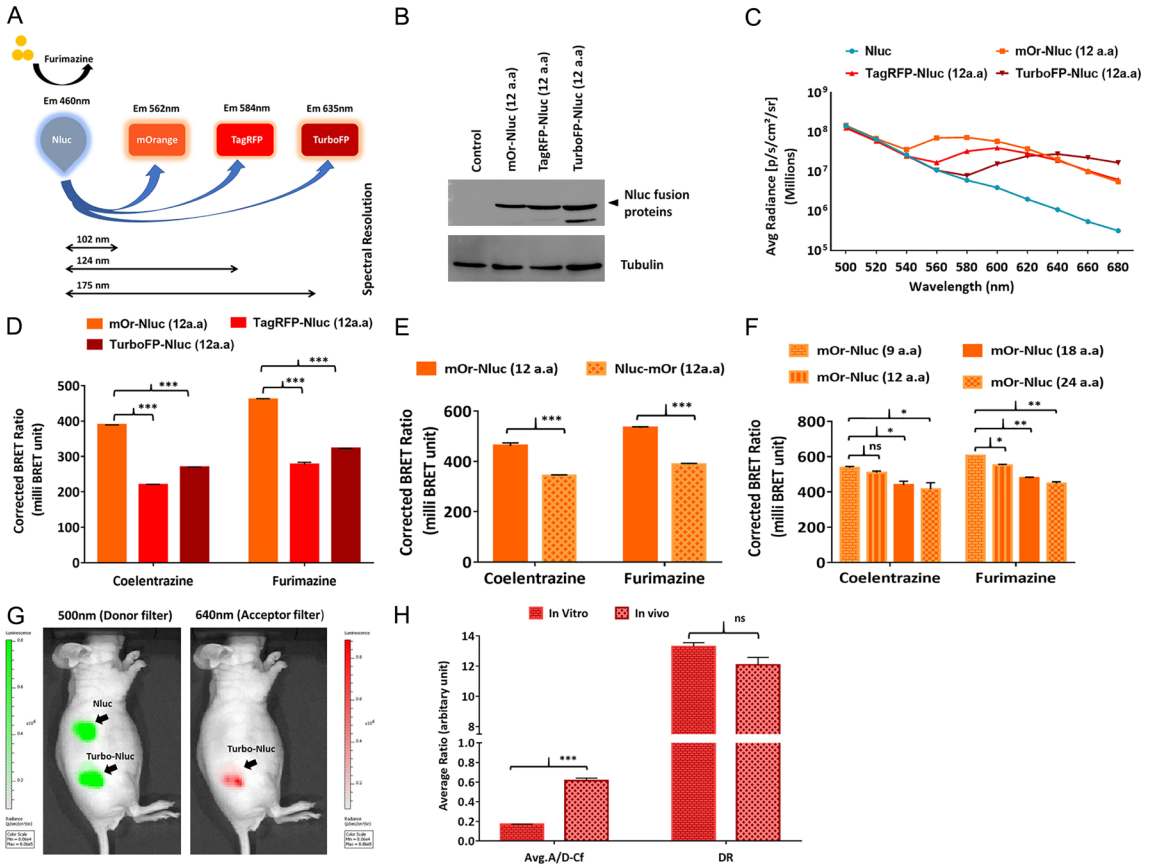

Figure 1. Development of Nanoluc based BRET system: A. Diagrammatic representation of spectral separation between Nluc (NanoLuc) emission and excitation maximum of different fluorophores in presence of furimazine substrate. B. Immunoblot of lysates from HT1080 cells expressing Nluc-fluorophores fusion proteins, probed with anti-RFP antibody. Upper band is the fusion protein in each case. Parental HT1080 cells were used as control. C. Spectral scan for Nluc fused with different fluorophores showing acceptor peak at respective filters (mOrange-560 nm, TagRFP-580 nm and TurboFP-640 nm) with Furimazine as substrate. D. Corrected BRET ratios (in milli BRET unit, mBU) for each of the Nluc-fluorophore fusion proteins in presence of two different substrates for Nluc (furimazine and coelenterazine). Spatial separation of 12 a.a. is kept constant between donor and acceptor in all fusion constructs. E. Graph representing the corrected BRET ratios for differentially oriented mOr-Nluc BRET pair. F. Effect of variable linker length from 9 a.a. to 24 a.a. on BRET ratio of mOr-Nluc (mBU) BRET pair. G. Representative image of nude mice implanted with HT1080 cells (3×10^6) stably expressing Nluc alone (top) and TurboFP-Nluc fusion protein (bottom) for *in vivo* BRET. Donor emission was collected at 500 nm filter and acceptor at 640 nm with 60 sec integration time per filter using furimazine as substrate. H. Graph representing comparison of corrected ratio (Avg.A/D-Cf) and double ratio calculated for both *in vitro* and *in vivo* BRET with Nluc and TurboFP BRET pair. All the above studies were done in HT1080 cells. Each graph represents mean ± SEM value, error bars represent SEM. Significance levels are *P<0.05, **P<0.01, and ***P<0.001 and ns for non-significant.

ange-Nluc; 460.72 mBU (furimazine) vs. 388.81 mBU (coelenterazine)] (**Figure 1D**). Overall, Nluc paired with mOrange showed the highest BRET efficiency using furimazine as a substrate when compared to other fluorophore acceptors.

Because energy transfer efficiency significantly relies on the geometric orientation of donor-acceptor moieties, fusion constructs of mOrange with Nluc were developed in different dipole orientations and transfected in HT1080 cells. Over here, Nluc oriented at the C-terminus (533 mBu) by the virtue of closest proximity shows significantly higher efficiency (P<0.001) of non-radiative energy transfer to mOrange as compared to the N-terminal orientation (388 mBu±0.0347), even with two different substrates (**Figure 1E**). Another important parameter that impacts BRET efficiency is the linker length between the donor and acceptor molecule. To verify this, constructs of Nluc separat-

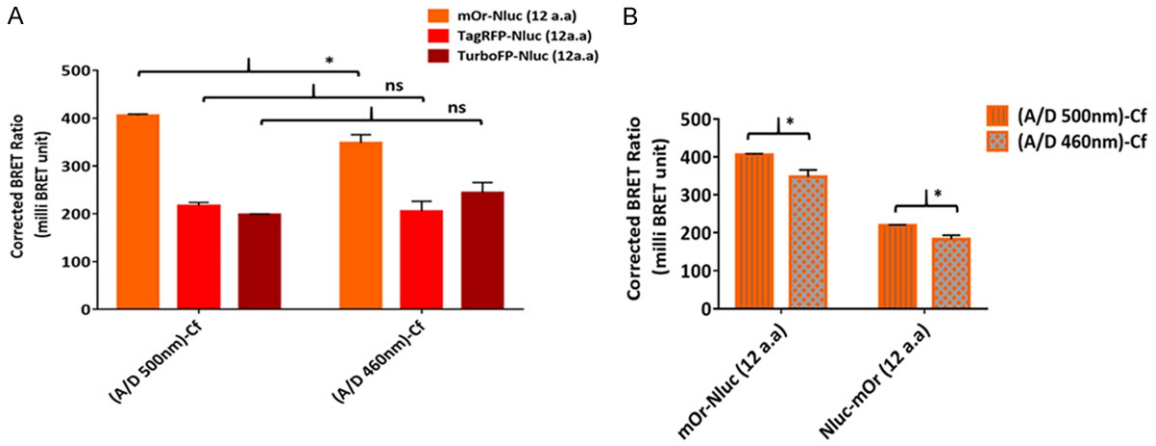

Figure 2. Comparison of BRET ratios using different donor channels for NanoLuc. A. Comparison of corrected BRET ratios obtained for mOrange-Nluc, TagRFP-Nluc or TurboFP-Nluc BRET pairs using different donor filters, 460 nm and 500 nm, in Cytation5 luminescence microplate reader. For all studies furimazine substrate was used. B. BRET ratio comparison done for N- or C-terminally tagged Nluc and mOrange BRET pairs using 500 nm or 460 nm donor filter. Each graph represents mean ± SEM value, error bars represent SEM. Significance levels are *P<0.05, ns indicates non-significant.

ed from mOrange with a variable GGS linker repeat sequence (9 a.a. to 24 a.a.) were expressed in HT1080 cells. With the difference in linker length from 9 a.a. to 12 a.a. (606.27 mBu and 550 mBu respectively) the RET efficiency of Nluc for mOrange majorly remains unaffected, however with further increment of linker length from 18 a.a. to 24 a.a. the corrected BRET ratios (478 mBu and 447 mBu respectively) drop significantly (P<0.01) (**Figure 1F**). Hence, C-terminal orientation of donor and N-terminal orientation of acceptor with an optimal linker length of 9-12 amino acids were considered, which also creates sufficient distance for protein folding in 3D conformation state for all control BRET pairs.

After obtaining a valid BRET pair using Nluc and TurboFP (emission maxima beyond 600 nm) combination *in vitro*, next we explore the potential of this pair to detect PPIs in deep tissues by performing *in vivo* BRET. HT1080 cells stably expressing either Nluc alone or TurboFP-Nluc fusion protein were injected subcutaneously onto the dorsal right flank of nude mice and imaged at respective donor (500 nm)-acceptor (640 nm) filter pairs (**Figure 1G**) Due to drastic difference in attenuation of signal for short wavelength emission, the bleed through subtracted corrected ratios (Avg. A/D-Cf) obtained for *in vivo* BRET (0.614 mBU) were 3-fold higher as compared to *in vitro* BRET (0.169 mBU, P<0.001). Hence double ratios were calculated (DR) that considerably minimized the effect of tissue attenuation on BRET measurements [20], as the latter is independent of total attenuation coefficient (**Figure 1H**). Similar DRs obtained both in case of mice (13.30 mBU) and cell culture BRET (12.07 mBU, P<0.05) confirms the ability of Nluc-TurboFP pair for sensitive detection of protein interactions even with deep tissue imaging in living subjects. Point to be noted here is that BRET ratios calculated using two different donor channels available on plate reader (i.e. 460±20 nm vs. 500±20 nm) show no significant difference in the BRET measurement efficiency (**Figure 2A**, **2B**). Therefore, even though Nluc-furimazine emission peak is at 460 nm, for BRET measurements done using IVIS spectrum, the 500 nm donor channel was used.

NanoLuc-TurboFP635 STAT3 BRET biosensor is a definite model for capturing STAT3 phosphorylation kinetics from live cells

Because of bright and stable luminescence from Nluc and high spectral resolution along with feasibility to be adopted for *in vivo* imaging with TurboFP made them an obvious choice for development of STAT3 phosphorylation driven homodimerization sensor (**Figure 3A**). Hence, fusion constructs of STAT3 either with Nluc donor or TurboFP acceptor were established in both the orientations (N- and C-terminus) with a

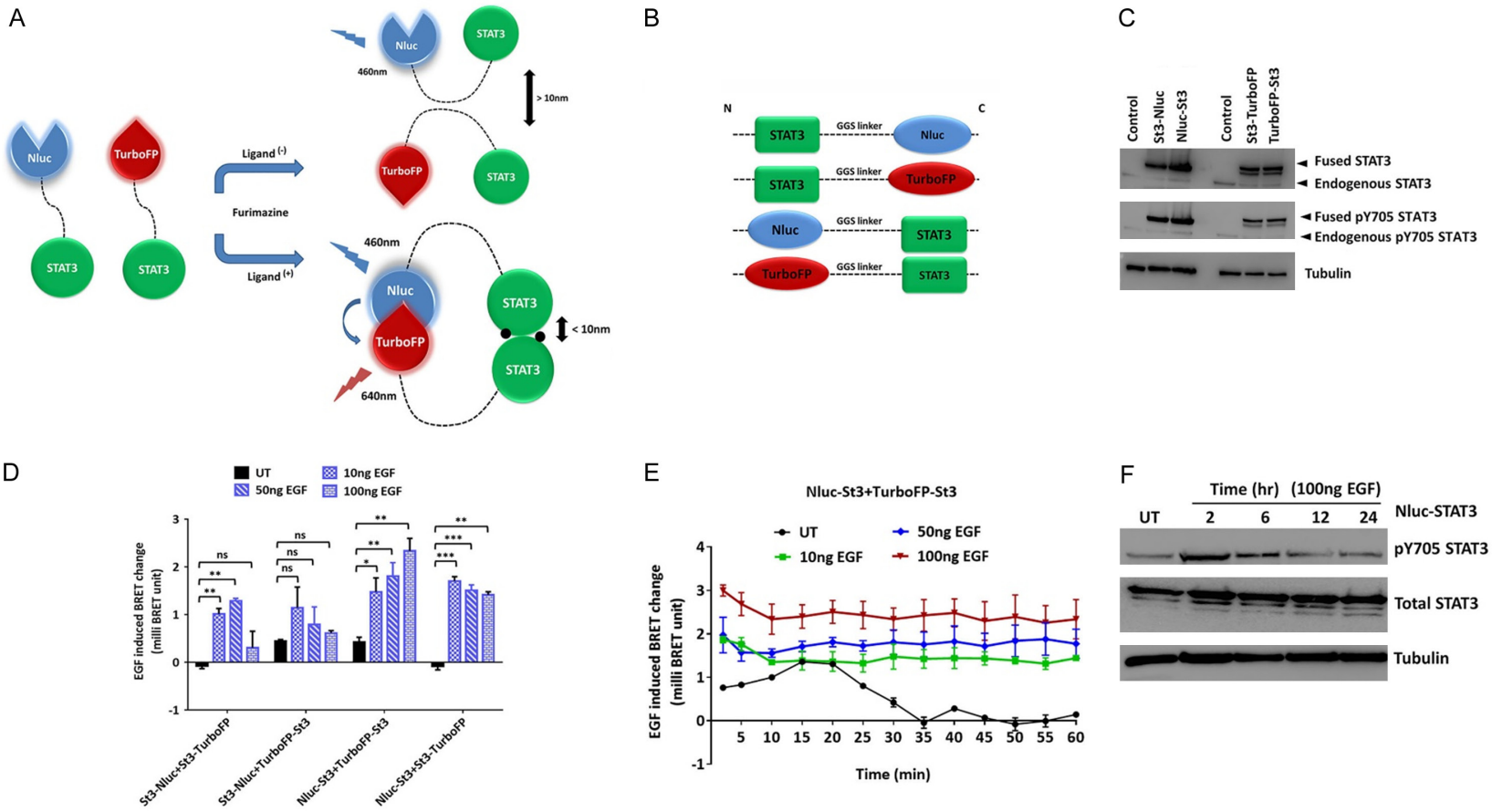

Figure 3. Development of STAT3 phosphorylation biosensor using Nluc and TurboFP BRET pair: A. Working model of STAT3 BRET sensor; STAT3 fused to either donor (Nluc) or acceptor (TurboFP) in the presence of substrate and ligand (that triggers activation and PTM of STAT3) undergoes dimerization and achieve a molecular distance less than 10 nm that allows energy from excited donor to be transferred to acceptor molecule. While in the absence of ligand or presence of inhibitor the two STAT3 molecules are far apart from each other allowing only donor signal to be detected without any energy transfer to the acceptor molecule. B. Schematic representation of all the four STAT3 BRET fusion constructs in different orientations. C. STAT3 BRET constructs transiently transfected in HT1080 cells shows expression of total STAT3 and activated from pY705-STAT3 along with the endogenous STAT3 pool. Upper band in each blot is the band of interest. D. Graph representing corrected BRET ratios (mBU) calculated for differentially oriented STAT3 BRET constructs transiently expressed in HT1080 cells at 30 mins post EGF treatment. E. Time kinetics graph (mBU) of BRET ratios for Nluc-St3+TurboFP-St3 BRET constructs transfected in HT1080 cells and stimulated with varying EGF concentration (0-100 ng). F. Immunoblot for time dependent phosphorylation and activation status of Nluc-St3 BRET fusion protein in response to EGF treatment (100 ng/ml). Phosphorylation is detected by probing for pY705 STAT3 and total STAT3 is determined by probing with anti-Nluc antibody in HT1080 cells. For all BRET studies Nanoluc activity was measured at 500 nm and for TurboFP at 640 nm in IVIS spectrum using furimazine as substrate. Each graph represents mean ± SEM value, error bars represent SEM. Significance levels are *P<0.05, **P<0.01, ***P<0.001 and ns as non-significant.

10 a.a. GGS linker separation and subjected to primary functional validation for proper protein formation (**Figure 3B**). Overexpression of these constructs in HT1080 cells and immunoblotting for total and pY705 STAT3 level confirms fusion protein translation and the ability to undergo spontaneous phosphorylation with endogenous cellular machinery (**Figure 3C**). In order to select an appropriate dipole orientation of STAT3 (ST3) BRET constructs where dimerization-driven BRET signal gain is maximum, a total of four probable combinations i.e. Nluc-ST3+TurboFP-ST3, Nluc-ST3+ST3-TurboFP, ST3-Nluc+ST3-TurboFP and ST3-Nluc+TurboFP-ST3 were established. Activation levels in each set were assayed by treatment with varying EGF concentrations (10-100 ng/ml) in comparison to serum-starved untreated cells and BRET ratios were calculated as described in Materials and Method section. Upon expression of these fusion constructs in HT1080 cells, treatment with the EGF ligand triggers an immediate response with a rapid increase in BRET signal within 5 min. A stable BRET signal is observed for upto 1 hour, for all the fusion combinations. However, of all the orientations tested, C-terminally oriented STAT3 BRET constructs (Nluc-ST3+TurboFP-ST3; 2.33 mBu, $P<0.01$ for 100 ng EGF) clearly stands out exhibiting a dose-dependent (10-100 ng EGF) significant gain in STAT3 activation and a subsequent increase in BRET signal (**Figure 3D**, **3E**). Additionally, to ensure that the gain in Phospho-BRET signal upon EFG treatment is a result of preceding phosphorylation event, Nluc-ST3 fusion expressing HT1080 cells were treated with EGF for different time points and pY705 activation levels were determined. As expected, EGF stimulation initiates Nluc-ST3 pY705 phosphorylation that drops down to basal level after 24 hrs (**Figure 3F**). This indicates that the fusion STAT3 is able sense the ligand trigger from cellular environment and can initiate the STAT3 signalling independently.

Further, in an attempt to achieve higher BRET signal, stable HT1080 cell line overexpressing acceptor-STAT3 fusion was established (**Figure 4A**). With constitutive expression of this fusion partner enhanced the BRET efficiency further. The result indicates that a BRET ratio of 1.57 mBU ($P<0.05$) obtained when acceptor stable cell population is transiently co-expressed for the donor-STAT3 combinations and incubated with only 10 ng EGF ligand. Point that also to be noted here is the Nluc-ST3 and Turbo-ST3 combination shows the highest BRET efficiency (1.61 mBu, $P<0.05$) when incubated with 100 ng EGF ligand (**Figure 4B**, **4C**). Hence, based on the above observations, donor/acceptor constructs with C-terminally orientated STAT3 were selected as final pair for further experiments.

STAT3 Phospho-BRET biosensor can detect STAT3 activation and dimerization in different cancer cell lines and with multiple ligands

Following the identification of Nluc/Turbo-STAT3 as optimal dipole orientation, we next sought to verify the applicability of developed BRET sensor as a working model to judge STAT3 activation across different cancer cell types and against variable pathway ligands. To achieve this, we transiently overexpressed the STAT3 Phospho-BRET sensor in a panel of multiple cancer cell lines including; MCF7 (breast cancer), HT1080 (Fibrosarcoma), PC3 (Prostate cancer), A549 (Adenocarcinomic human alveolar basal epithelial cells) cells and challenged with IL6 at variable concentration, another potential ligand of STAT3 pathway. Despite having a differential biological milieu, the STAT3 Phospho-BRET sensor sensitively captures the activation phenomenon, upon ligand stimulation across all the model cancer cell lines tested (HT1080 [2.14 mBU, $P<0.01$], PC3 [2.3 mBU, $P<0.05$], MCF7 [1.57 mBU, $P<0.05$] and A549 [4.43 mBU, $P<0.01$] for 10 ng IL6) (**Figure 5A-E**). PC3 being a STAT3 null (**Figure 5D**) and HT1080/A549/MCF7 being STAT3 positive, the compounding effect of variable endogenous STAT3 pool, also did not affect the strength of BRET signal achieved. Further, as expected the increment in BRET signal observed shows linear dependency upon ligand (IL6) concentration, except in case of MCF 7 cells. Surprisingly, pertaining to its potency, IL6 turned out to be a better ligand as it could achieve BRET ratio equivalent to EGF treatment (100 ng) with even 10-fold lower ligand concentration [for e.g. HT1080-10 ng IL6 (2.14 mBU) and 100 ng EGF (2.20 mBU)] (**Figure 5A**). These results clearly highlight the inherent strength of the STAT3 Phospho-BRET sensor to work as a sensing model irrespective of the genetic background of model cell line or stimulating ligand.

The differential BRET ratios achieved with the same EGF concentration (100 ng) across a panel of cancer cell lines, intrigued us to look for EGFR expression level. Over here, quantita-

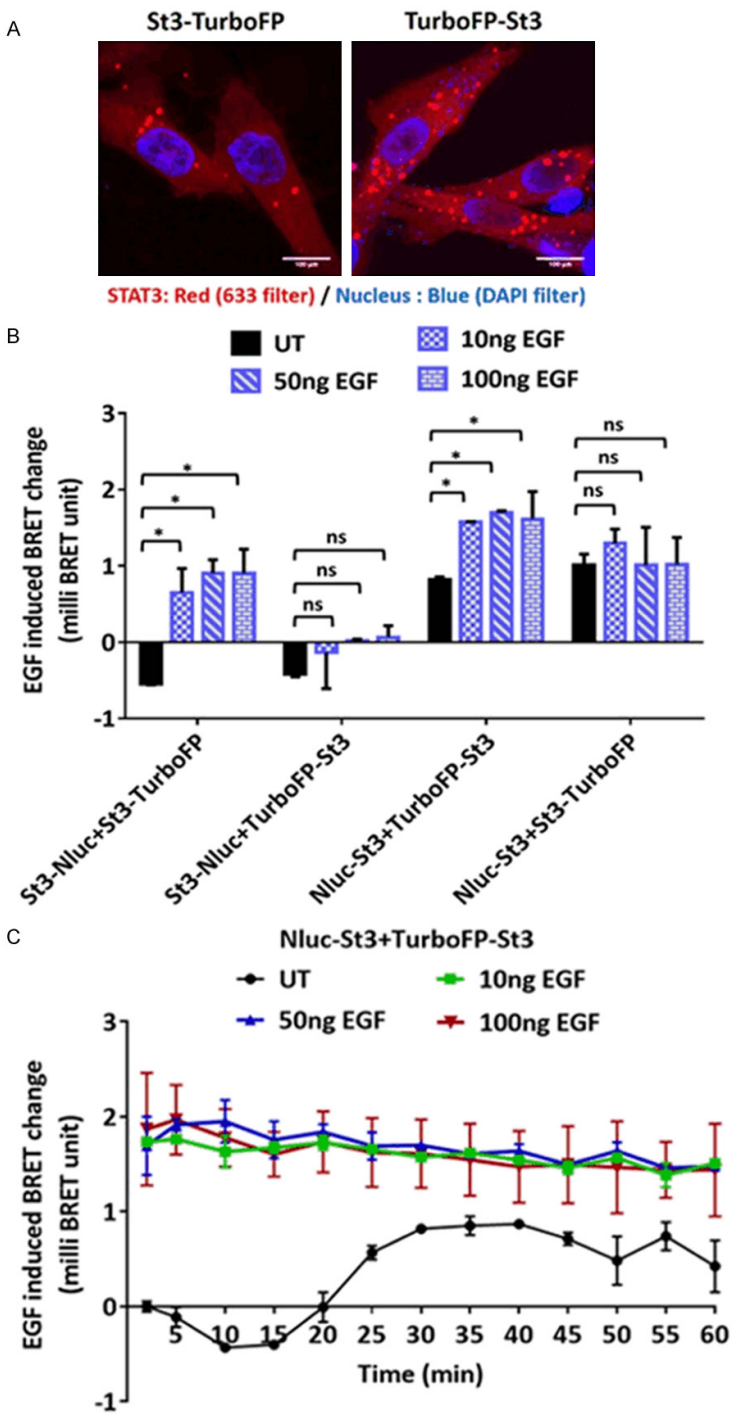

Figure 4. Activation kinetics of phospho-STAT3 BRET constructs in HT1080 acceptor stable cells in response to variable amount of EGF ligand. A. Fluorescence microscopy images of HT1080 cells stably expressing either the TurboFP-St3 or St3-TurboFP acceptor plasmids (uninduced). Nucleus is stained with DAPI and STAT3 signal was acquired at 633 nm filter for TurboFP. B. BRET ratios measured for differentially oriented donor-STAT3 constructs transiently expressed in acceptor-STAT3 stable background, post 30 min of EGF trigger. C. Dynamics of BRET ratios measured for Nluc-St3+TurboFP-St3 BRET construct for 60 min, post EGF induction at variable concentration (10 ng-100 ng) using furimazine as substrate. Nanoluc activity was measured at 500 nm and TurboFP at 640 nm filter at every 5 min for 1 hour. Y-axis represent corrected BRET ratio in milli BRET units (mBU) and X-axis represent time in minutes. Each graph represents mean ± SEM value, error bars represent SEM. Significance levels are *P<0.05, **P<0.01, ***P<0.001 and ns as non-significant.

tive assessment of EGFR transcript level with the BRET ratio gained in the respective cell line points towards the role of receptor density on cell surface as key factor influencing BRET signal (**Figure 5F**). Cells having high EGFR expression [e.g. A549, 4.17 mBU] respond more strongly to the same EGF concentration as compared to the low EGFR-expressing cell line [MCF7 (1.48 mBU) and HT1080 (2.20 mBU); 100 ng, P<0.05 and 0.01 respectively] (**Figure 5G**). Finally, to confirm the specificity of the sensor, prior blocking of EGF receptor with an EGFR neutralizing antibody in MCF7 cells successfully abrogates EGF-mediated STAT3 activation (1.15 mBU with EGF and 0.92 mBU with EGF+EGFR Ab, P<0.05) and a parallel attenuation in BRET signal gain (**Figure 5H**, **5I**). These data indicate that the activation response obtained with the STAT3 BRET sensor upon EGF treatment is a true event of EGF-EGFR mediated STAT3 phosphorylation and homodimerization. Collectively these observations clearly demonstrate the specificity and versatile nature of the developed STAT3 Phospho-BRET sensor as true representation of STAT3 activation events from live cell.

STAT3 Phospho-BRET biosensor is compatible for high-throughput screening of different STAT3 inhibitors

The need to find promising STAT3 inhibitors that can clear the

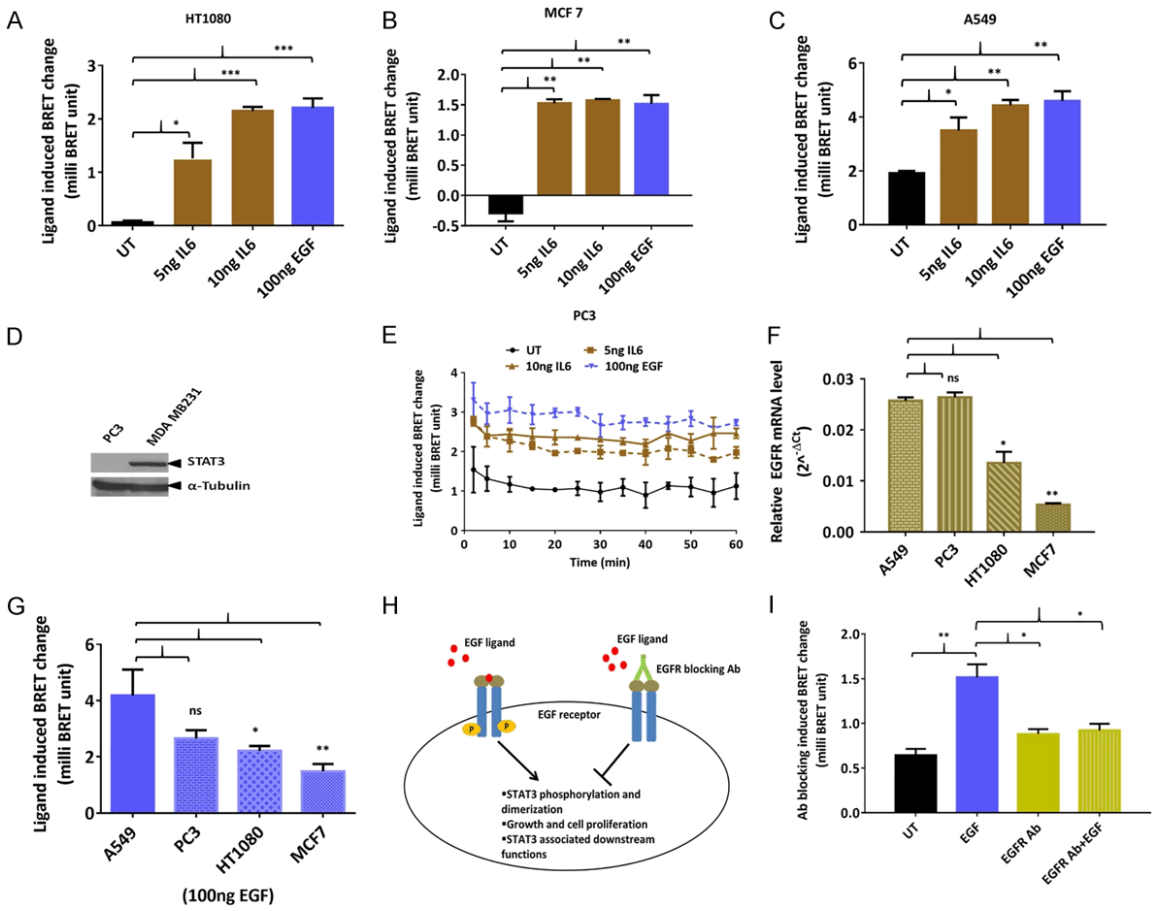

Figure 5. Specificity and sensitivity of phospho-STAT3 BRET biosensor: A. HT1080 cells transfected with Nluc-St3 and TurboFP-St3 wildtype BRET plasmids. Corrected BRET ratio graph (mBU) represent 30 min post ligand trigger condition with both IL6 and EGF as ligands. B, C. Representative graphs of corrected ratios (mBU) for MCF7 and A549 cells respectively showing activation of phospho-STAT3 BRET sensor 30 min post ligand trigger. D. Immunoblot of PC3 cells probed for endogenous STAT3 expression. MDA MB 231 cells were used as positive control. E. Kinetics of change in BRET ratio (mBU) in PC3 cells for STAT3 BRET sensor at varying ligand concentration. F. Relative EGFR mRNA level in different cancer cell lines tested. Normalization was done using GAPDH. G. Corrected BRET ratio values (mBU) for respective cancer cell lines expressing STAT3 BRET construct at 30 min post 100 ng EGF treatment. H. Schematic representation on mode of action of EGFR blocking antibody on STAT3 signaling. I. Representative graphs show corrected BRET ratios (mBU) for MCF7 cells expressing STAT3 BRET constructs either treated with or without EGFR blocking antibody in presence and absence of EGF (mean ± SEM, error bars represent SEM). Significance levels are *P<0.05, **P<0.01, ***P<0.001 and ns as non-significant.

clinical trials demands for a very robust and much more strategic approach in screening STAT3 inhibitors [22]. With the advantages shown by the developed STAT3 Phospho-BRET biosensor to precisely read modulations in the STAT3 pathway, we next sought to adapt it in HTS platform as a drug screening tool. For this, we performed BRET assays in MCF7 cells expressing genetically encoded STAT3 phospho-BRET sensor with relatively six-fold less adherent cell number in a 384-well plate and compared its sensitivity with a conventional 96 well plate format. A random screen of seven different compounds (either known or unknown STAT3 modulators) with differential concentrations either in absence or presence of EGF yield significant results. Out of the 7, four compounds [MS-275 (-0.157 mBU), Niclosamide (-0.287 mBU), Stattic (0.325 mBU) and Curcumin (-0.367 mBU) against EGF^+ (1.4 mBU)] shows significant attenuation in STAT3 activity despite giving EGF stimulation. While remaining three drugs [AR-42 (1.05 mBU), Chidamide (1.00 mBU) and CI994 (0. strategic 603 mBU) against EGF^+ (1.4 mBU)] though activated STAT3 but failed to achieve signal strength as equivalent

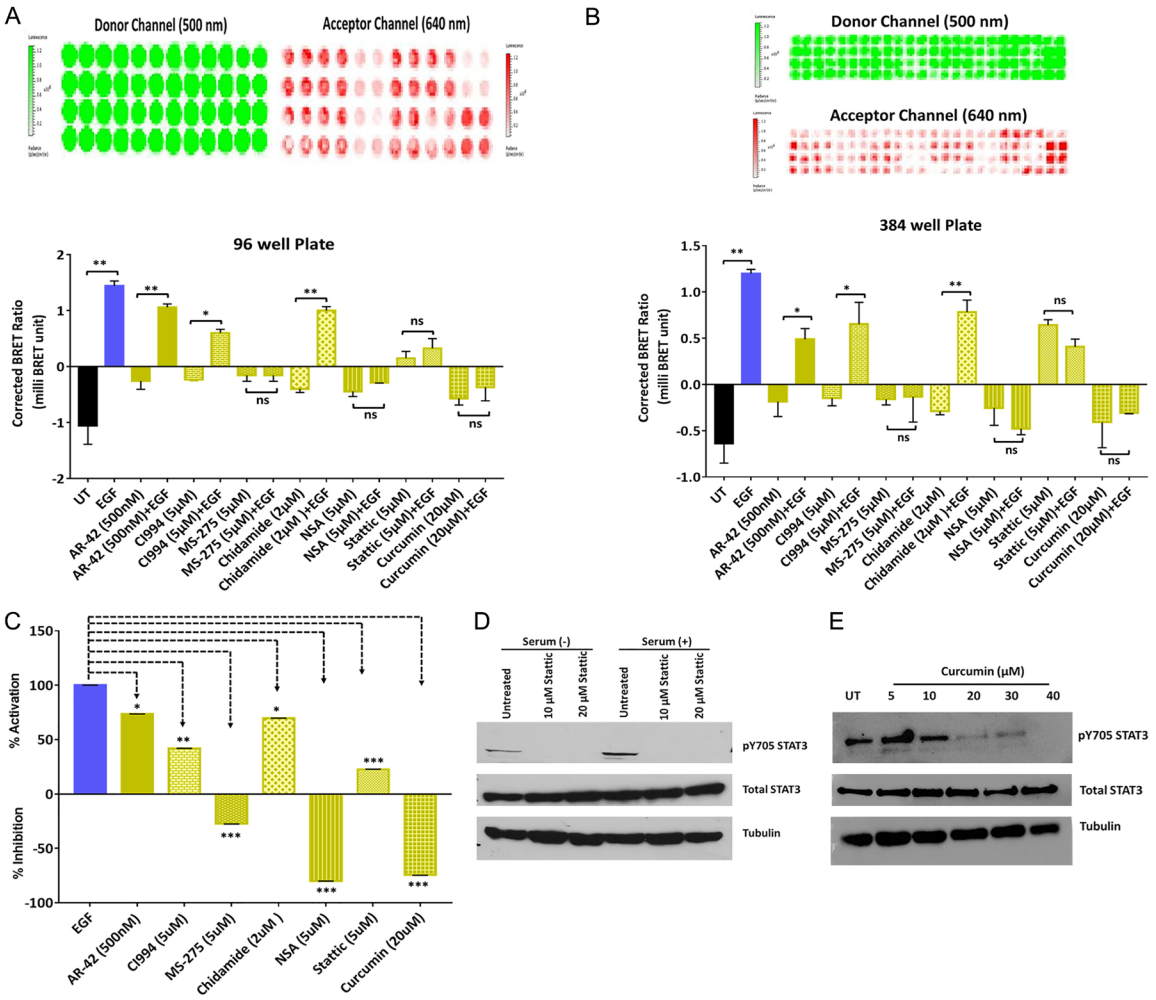

Figure 6. STAT3 Phospho-BRET biosensor is HTS compatible for STAT3 pathway inhibitor screen: A, B. Representative plate images of compound library screen using Phospho STAT3 BRET sensor in 96 and 384 black well plate, respectively, at specific donor and acceptor channels. Bottom graph in each case represents corrected ratios calculated for each drug concentration with or without EGF (100 ng). C. Percent inhibition or activation of BRET signal achieved with respect to EGF treated sample as control (100%). Percent activation is calculated by dividing corrected ratio of drug treated sample with EGF treated control *100. For percent inhibition the above calculated value is subtracted from 100. D, E. Immunoblot of MCF 7 cells treated with different concentrations of Stattic (either in serum positive or serum negative condition) and Curcumin, respectively. Each blot is probed for total and pY705 STAT3, with tubulin as loading control. Each bar represent mean ± SEM, error bars represent SEM. Significance levels are *P<0.05, **P<0.01, ***P<0.001 and ns as non-significant.

to EGF treated control (**Figure 6A**, **6B**). Surprisingly, of the inhibitory compounds identified, Curcumin (74% inhibition) [23] and niclosamide (80% inhibition) [24] were more potent than the previously well-known STAT3 inhibitor, Stattic (22% activation) [25], (**Figure 6C**). The reason for higher potency of both niclosamide and curcumin could be attributed to their ability to inhibit STAT3 activation by abrogating multiple other pathways that either directly or indirectly activate the STAT3 molecule [26, 27], while Stattic is more specifically a SH2 domain binder [25]. The remaining three compounds (i.e. Chidamide, CI-994 and AR-42), that show high BRET signal upon EGF trigger in the HTS screen were majorly HDAC inhibitors, that probably activated STAT3 by increasing overall acetylation of the genome with concomitant increase in inducers of STAT3 pathway [28].

While a majority of HTS assays rely on 96 well plate format, here we have shown that STAT3 phospho BRET sensor works even in 384 well

format while using the same imaging equipment for photonic quantification. A comparable bleed through subtracted BRET signal from two different plate formats (96 vs. 384) clearly shows uncompromised and sensitive signal detection ability of STAT3 phospho-BRET sensor despite adapting to the miniature platform. Finally, to confirm the STAT3 inhibitory mode of action for these drugs, Curcumin and Stattic were randomly selected as drug candidates from the BRET screen for *in vitro* validation. Here, treating MCF7 cells with differential doses of both Curcumin and Stattic (either in serum-positive or serum-starved conditions) respectively, shows a significant drop in activated pY705 STAT3 levels (**Figure 6D**, **6E**), thereby confirming loss of phosphorylation mediated drop in homodimerization signal as mechanistic basis for STAT3 Phospho-BRET sensor. Collectively, these results clearly demonstrate the ability of STAT3 Phospho-BRET sensor as a promising high-throughput, specific and multidrug screening tool against the oncogenic STAT3 pathway.

Conclusion

Pertaining to the excellent quantum efficiency, NanoLuc has form an efficient BRET donor for fluorophores such as mOrange, TagRFP and TurboFP with 100 nm or more spectral resolution and thus provide opportunity to work with BRET systems with minimal bleed through signal at donor and acceptor channel. For the TurboFP-Nluc pair, the furimazine substrate yields a reasonably higher BRET ratio (351.5 mBU) than a value when coelenterazine substrate is used (296.6 mBU). Considering the reasonable dynamic range obtained from TurboFP-Nluc BRET pair, alongside of its suitability for non-invasive molecular imaging, we have utilized this new BRET combination for developing a BRET biosensor that provides the monitoring ability of dynamic STAT3 phosphorylation directly from live cells in culture. STAT3, being an important oncogenic signalling pathway, it is a prime target for therapeutic intervention [29]. However, one of the major challenges is the lack of an appropriate assay system to help screen the inhibitors for their specific action against STAT3 signalling in the live cell environment. Though virtual screening and structure-based drug designing approaches strongly pave the path for identifying novel compounds, final validation both *in vitro* and *in vivo* is mandatory [30]. The STAT3 Phospho-BRET biosensor system is developed to bridge this technological gap, where as a measure of an immediate effect of protein phosphorylation, STAT3 forms homodimer, resulting in increased BRET ratio. After careful optimization of the dipole angular orientation, STAT3 placed at the C-terminus end of both the donor and the acceptor moiety is found to be the best orientation. Alongside of a thorough validation of this biosensor, we have further tested it for revealing the capacity to report real-time phosphorylation events occurring *in situ* using EGF and IL6 ligands in different types of cancer cells.

Pertaining to its ability to give a true read out of the STAT3 activation event, irrespective of either the genetic background of the cell model or differential ligand modulators (e.g. IL6 and EGF), this assay system holds true potentials of deciphering STAT3 biology. The biosensor is also expected to provide novel and specific measures of a range of compounds with inhibitory action on STAT3 signalling directly from live cells. Here, as a token measure of the HTS compatibility of the biosensor, we have shown that signal strength is equally sensitive in 96 well plate with 20 K cells vs. 384 well plate with only 5 K cells. Thus, in future this technology can be used for studying role of key post translational modifications in changing the dimerization status of STAT3 and screening potential inhibitors against this very important transcriptional regulatory protein involved in various oncogenic pathways.

Acknowledgements

The authors acknowledge funding support from Department of Biotechnology (DBT)-Bioengineering project [REF NO. BT/PR3651/MED/32/210/2011], Govt. of India, New Delhi and ACTREC for facilities. We acknowledge Promega for generously providing us with the NanoLuc plasmid and antibody.

Disclosure of conflict of interest

None.

Address correspondence to: Dr. Abhijit De, Molecular Functional Imaging Lab, Advanced Centre for Treatment, Research and Education in Cancer (ACTREC), Tata Memorial Centre, Sector 22, Kharghar,

Navi Mumbai 410210, India. Tel: +91-22-2740 5038; Fax: +91-22-2740 5085; E-mail: ade@actrec.gov.in

References

[1] Paulmurugan R and Gambhir SS. Novel fusion protein approach for efficient high-throughput screening of small molecule-mediating protein-protein interactions in cells and living animals. Cancer Res 2005; 65: 7413-7420.

[2] Berggård T, Linse S and James P. Methods for the detection and analysis of protein-protein interactions. Proteomics 2007; 7: 2833-2842.

[3] De A. The new era of bioluminescence resonance energy transfer technology. Curr Pharm Biotechnol 2011; 12: 558-568.

[4] De A, Rohit A and Jasani A. Engineering aspects of bioluminescence resonance energy transfer systems. in: Cai W, editor. Engineering in Translational Medicine. London: Springer; 2014. pp. 257-300.

[5] England CG, Ehlerding EB and Cai W. NanoLuc: a small luciferase is brightening up the field of bioluminescence. Bioconjug Chem 2016; 27: 1175-1187.

[6] Zhao J, Nelson TJ, Vu Q, Truong T and Stains CI. Self-assembling NanoLuc luciferase fragments as probes for protein aggregation in living cells. ACS Chem Biol 2016; 11: 132-138.

[7] Machleidt T, Woodroofe CC, Schwinn MK, Mendez J, Robers MB, Zimmerman K, Otto P, Daniels DL, Kirkland TA and Wood KV. NanoBRET--a novel BRET platform for the analysis of protein-protein interactions. ACS Chem Biol 2015; 10: 1797-1804.

[8] Salahpour A, Espinoza S, Masri B, Lam V, Barak LS and Gainetdinov RR. BRET biosensors to study GPCR biology, pharmacology, and signal transduction. Front Endocrinol (Lausanne) 2012; 3: 105.

[9] Song G, Wu QP, Xu T, Liu YL, Xu ZG, Zhang SF and Guo ZY. Quick preparation of nanoluciferase-based tracers for novel bioluminescent receptor-binding assays of protein hormones: using erythropoietin as a model. J Photochem Photobiol B 2015; 153: 311-316.

[10] Zhang L, Song G, Xu T, Wu QP, Shao XX, Liu YL, Xu ZG and Guo ZY. A novel ultrasensitive bioluminescent receptor-binding assay of INSL3 through chemical conjugation with nanoluciferase. Biochimie 2013; 95: 2454-2459.

[11] Lackner DH, Carré A, Guzzardo PM, Banning C, Mangena R, Henley T, Oberndorfer S, Gapp BV, Nijman SMB, Brummelkamp TR and Bürckstümmer T. A generic strategy for CRISPR-Cas9-mediated gene tagging. Nat Commun 2015; 6: 10237.

[12] Yasuzaki Y, Yamada Y, Ishikawa T and Harashima H. Validation of mitochondrial gene delivery in liver and skeletal muscle via hydrodynamic injection using an artificial mitochondrial reporter DNA vector. Mol Pharm 2015; 12: 4311-4320.

[13] Shalini D and De A. Approaching non-canonical STAT3 signaling to redefine cancer therapeutic strategy. Integr Mol Med 2017; 4: 10.

[14] Matsuno K, Masuda Y, Uehara Y, Sato H, Muroya A, Takahashi O, Yokotagawa T, Furuya T, Okawara T, Otsuka M, Ogo N, Ashizawa T, Oshita C, Tai S, Ishii H, Akiyama Y and Asai A. Identification of a new series of STAT3 inhibitors by virtual screening. ACS Med Chem Lett 2010; 1: 371-375.

[15] Schroder M, Kroeger KM, Volk HD, Eidne KA and Grütz G. Preassociation of nonactivated STAT3 molecules demonstrated in living cells using bioluminescence resonance energy transfer: a new model of STAT activation? J Leukoc Biol 2004; 75: 792-797.

[16] Lacey VK, Parrish AR, Han S, Shen Z, Briggs SP, Ma Y and Wang L. A fluorescent reporter of the phosphorylation status of the substrate protein STAT3. Angew Chem Int Ed Engl 2011; 50: 8692-8696.

[17] Kretzschmar AK, Dinger MC, Henze C, Brocke-Heidrich K and Horn F. Analysis of Stat3 (signal transducer and activator of transcription 3) dimerization by fluorescence resonance energy transfer in living cells. Biochem J 2004; 377: 289-297.

[18] Dabir S, Kluge A and Dowlati A. The association and nuclear translocation of the PIAS3-STAT3 complex is ligand and time dependent. Mol Cancer Res 2009; 7: 1854-1860.

[19] Dimri S, Basu S and De A. Use of BRET to study protein-protein interactions in vitro and in vivo. Methods Mol Biol 2016; 1443: 57-78.

[20] Dragulescu-Andrasi A, Chan CT, De A, Massoud TF and Gambhir SS. Bioluminescence resonance energy transfer (BRET) imaging of protein-protein interactions within deep tissues of living subjects. Proc Natl Acad Sci U S A 2011; 108: 12060-12065.

[21] De A, Jasani A, Arora R and Gambhir SS. Evolution of BRET biosensors from live cell to tissue-scale in vivo imaging. Front Endocrinol (Lausanne) 2013; 4: 131.

[22] Wake MS and Watson CJ. STAT3 the oncogene-still eluding therapy? FEBS J 2015; 282: 2600-2611.

[23] Hahn YI, Kim SJ, Choi BY, Cho KC, Bandu R, Kim KP, Kim DH, Kim W, Park JS, Han BW, Lee J, Na HK, Cha YN and Surh YJ. Curcumin interacts directly with the Cysteine 259 residue of STAT3 and induces apoptosis in H-Ras transformed human mammary epithelial cells. Sci Rep 2018; 8: 6409.

[24] Shi L, Zheng H, Hu W, Zhou B, Dai X, Zhang Y, Liu Z, Wu X, Zhao C and Liang G. Niclosamide inhibition of STAT3 synergizes with erlotinib in human colon cancer. Onco Targets Ther 2017; 10: 1767-1776.
[25] Schust J, Sperl B, Hollis A, Mayer TU and Berg T. Stattic: a small-molecule inhibitor of STAT3 activation and dimerization. Chem Biol 2006; 13: 1235-1242.
[26] Tomeh MA, Hadianamrei R and Zhao X. A review of curcumin and its derivatives as anticancer agents. Int J Mol Sci 2019; 20.
[27] Li Y, Li PK, Roberts MJ, Arend RC, Samant RS and Buchsbaum DJ. Multi-targeted therapy of cancer by niclosamide: a new application for an old drug. Cancer Lett 2014; 349: 8-14.
[28] Eckschlager T, Plch J, Stiborova M and Hrabeta J. Histone deacetylase inhibitors as anticancer drugs. Int J Mol Sci 2017; 18.
[29] Sellier H, Rébillard A, Guette C, Barré B and Coqueret O. How should we define STAT3 as an oncogene and as a potential target for therapy? JAKSTAT 2013; 2: e24716.
[30] Yuriev E. Challenges and advances in structure-based virtual screening. Future Med Chem 2014; 6: 5-7.